Pol. J. Environ. Stud. Vol. 32, No. 4 (2023), 3883-3893
DOI: *10.15244/pjoes/166158* ONLINE PUBLICATION DATE: 2023-06-19

Original Research

Carbonized Waste Cation Exchange Resin with Fe Doping for Persulfate Activation and Oxytetracycline Degradation: Performance and Mechanism

Kun Yang[1, 2], Qiang Li[1, 2]*, Huiyuan Deng[3], Dongsheng Xia[1, 2]

[1]School of Environmental Engineering, Wuhan Textile University, Wuhan 430073, PR China
[2]Engineering Research Center for Clean Production of Textile Dyeing and Printing, Ministry of Education, Wuhan 430073, China
[3]Institute of Spatial Planning of Hubei Province, Wuhan, 430064, China

Received: 15 March 2023
Accepted: 15 May 2023

Abstract

To resource utilization of the spent cation exchange resin, the carbonized resin with Fe doping (Fe_3O_4@CR) was prepared to activate persulfate (PS) for the degradation of oxytetracycline (OTC). Fe_3O_4@CR exhibited high catalytic potential for the degradation of OTC with relatively low activation energy (E_a = 28.86 kJ/mol). In the Fe_3O_4@CR/PS system, 76.4% of the OTC was removed under the conditions ([PS]: 0.15 g/L, [Fe_3O_4@CR]: 0.3 g/L, T: 25ºC). Fe_3O_4@CR could work effectively for activating PS to degrade OTC in the pH range of 3.0-7.0. The free radical quenching experiments and electron paramagnetic resonance (EPR) analysis showed that $^{\bullet}OH$ and $SO_4^{\bullet-}$ were the main radicals for the degradation of OTC. The conversion between Fe^{3+} and Fe^{2+} accelerated the degradation of OTC by generating $^{\bullet}OH$ and $SO_4^{\bullet-}$. The possible degradation pathways were proposed. The OTC was mineralized to smaller molecules, such as $C_{14}H_{10}O_3$ and $C_7H_{11}O$. This study offers a new perspective on waste resin recycling and water purification.

Keywords: resin, carbonized, persulfate, degradation, mechanism

Introduction

With the development of society, antibiotics have been widely used in human and animal bacterial infections [1]. Due to their limited biodegradability, they can be detected in soil, surface water, and surface sediments [2]. Oxytetracycline (OTC) is a tetracycline antibiotic with a broad range of action. Because of its inexpensive cost and therapeutic impact, OTC is commonly utilized in aquaculture and animal husbandry. Once OTC is extensively used and not properly treated, the residual OTC will harm the ecological environment [3]. The issues contain bacterial resistance and resistance genes. Therefore, the impact of antibiotic resistance on human health needs to be

*e-mail: qiangli@wtu.edu.cn

further addressed. And the removal of OTC from the environment has attracted much attention.

At present, a variety of technologies can remove antibiotics, such as biological treatment, adsorption, chemical oxidation treatment, etc [4]. Because antibiotics have the effect of inhibiting bacteria, the overall efficiency of biological treatment technology is low [5]. The adsorbent can realize the separation of the antibiotics in the wastewater, but the concentrated solution requires further treatment [6]. Chemical oxidation treatment has become more promising in the treatment of antibiotic wastewater because of its good chemical stability and low operating cost [7]. Persulfate-based advanced oxidation (PS-based AOPs) can degrade organic compounds by activating to generate radicals, such as sulfate radicals ($SO_4^{\bullet-}$) and hydroxyl radicals (•OH) [8]. PS-based AOPs own great potential application for water treatment and the activation of PS is extremely significant [9].

Transition metal, such as Fe, Ni, Ce, Co, Mn, and Cu has exhibited more cost-effective activation than high-energy activation methods (thermal, UV radiation, etc.) [10, 11]. Fe-based activator has attracted much attention due to their low toxicity, geological reserves, and easy recovery, such as zero-valent iron [12], Fe_3O_4 [13], Fe-Fe_2O_3 [14], Fe-carbon [15], etc. Fe-carbon materials could be used as activators by being prepared from various carbon precursors, such as coconut shells [16], balsa woods [17], and waste resins [18]. Among these, carbon materials from carbonized waste resins as activators can realize the recycling treatment of waste resin.

Cation exchange resins are widely used for the removal of metal ions from industrial water [19]. However, further treatment of the saturated resin is required during use. After long-term reuse, the resin may lose its function and turn into waste resin. Reasonable disposal of the spent resin and reducing the impact on the environment is an urgent issue. Several studies attempted to recycle the spent resin by carbonizing them as a persulfate activator [20]. Shi et al. used waste ion exchange resin to prepare iron-immobilized resin chars and activated PS for the degradation of Orange G [21]. In addition, Liu et al. synthesized carbon-supported Co from waste resin for the activated PMS degradation of trimethoprim [22]. Yang et al. prepared the carbon-supported Fe-Co bimetal material by carbonization and showed superior activation performance for peroxymonosulfate to degrade atrazine [18]. However, the research on the structural properties of the carbonized resin still needs further study. The activated performance and mechanism after resin carbonized with Fe doping were also unclear.

In the study, the waste cation exchange resin was carbonized with Fe doping and its degradation of OTC by activating PS was investigated. The structure of Fe_3O_4@CR was characterized. The effect of operating conditions such as catalyst dosage, PS dosage, initial pH, and coexisting pollutants on catalytic performance was studied and the reusability of Fe_3O_4@CR was also performed. Finally, the free radical degradation pathway and the specific formation mechanism of OTC were explored, and the intermediates in the degradation process and the mineralization process were described.

Material and Methods

Materials and Chemicals

The waste cation exchange resin (D001) was obtained from the laboratory. Sodium hydroxide (NaOH), tert-butyl alcohol (TBA), sodium persulfate (PS), 2,2,6,6-tetramethyl-4-piperidone (TEMP), and 5,5-dimethyl-1-pyrroline N-oxide (DMPO) were provided by Aladdin Chemical Company. Oxytetracycline (OTC), ferrous sulfate, methanol (MeOH), sodium sulfate, sodium bicarbonate, sodium carbonate, and monopotassium phosphate were provided by Sinopharm Chemical Reagent Co. Ltd. Potassium bromide was purchased from Rhawn Chemical Technology Co. Ltd. Chloroform (Chlor) was purchased from Shanghai Yien Chemical Technology Co. Ltd. The L-histidine was provided by Regal Science & Technology Co. Ltd.

Synthesis of Fe_3O_4@CR and Carbonized Resin (CR) Catalyst

The waste resin (D001) was washed with deionized water and ethanol at a dosage of 3.0 g. After washing, the resin was ground and sieved with a 300-mesh sieve. The sieved powdered resin was soaked in ferrous sulfate solution (25 g/L) for 8 h. After separation, the composite material was dried at 50ºC. The composite material was calcined for 60 min at 450ºC by a muffle furnace. After washing and drying, the catalyst (Fe_3O_4@CR) was obtained. Fe_3O_4 was prepared by further calcining Fe_3O_4@CR at 500ºC for 6 h. According to the same steps above (except soaking), carbonized resin (CR) was obtained after the powdered resin was calcined for 60 min at 450ºC by a muffle furnace.

Experimental Procedure

100 mL of OTC solution (20 mg/L), the appropriate amount of catalyst and PS were added into a 250 mL conical flask and the catalytic reaction was carried out. 1 mL of the sample was obtained at predetermined intervals and quenched with methanol. After centrifugation, the concentration of the sample was analyzed. In the experiment of the pH effect on the degradation, the pH of the reaction solution was adjusted to 3.0, 5.0, 7.0, 9.0, and 11.0 using 0.05 M hydrochloric acid and sodium hydroxide. The coexisting ions Cl^-, SO_4^{2-}, HCO_3^-, $H_2PO_4^-$, and CO_3^{2-} (1 mM, 5 mM, 10 mM) were added to investigate the effect

on the degradation. MeOH (10 mM) and TBA (10 mM) were used to verify the sulfate radicals ($SO_4^{\bullet-}$) and hydroxyl (HO•), L-histidine (1 mM) and Chlor (1 mM) were used to identify singlet oxygen ($^1O_2$) and superoxide anion radical ($O_2^{\bullet-}$). The Fe_3O_4@CR was collected with a magnet and washed clean with deionized water during repeated cycling experiments. A single experiment was repeated twice to ensure the accuracy of the experimental data.

Characterization

The morphology of the catalyst was examined by scanning electron microscopy (FE-SEM, Zeiss Sigma HD, USA), and its magnetic characteristics were determined by measurement of physical properties (PPMS-9, Quantum Design Inc., USA). Then, X-ray diffraction patterns (XRD, Bruker D8 boost, Germany) as well as Fourier transform infrared spectroscopy (FT-IR, Bruker Vertex 70, Germany) was used to identify the crystal structure and functional groups of the catalyst.

Analysis Methods

The total organic carbon analyzer (TOC-2000, Shimadzu, Japan) and EPR instrument (EPR, Bruker Model A300-10/12, Germany) were used to analyze the OTC mineralization rate and identify the free radicals of Fe_3O_4@CR/PS system. UV spectrophotometer (UV-2000, Mapada, China) and HPLC-MS/MS system (Ultimate 3000 UHPLC-Q Exactive, US) were used to analyze the OTC concentration and detect the degradation intermediates during the degradation, respectively. In addition, the reaction rate for the first 40 min was fitted with the aid of a pseudo-first-order equation.

$$\ln (C_0/C_t) = k_{obs}\, t \quad (1)$$

In the above formula, when the reaction time is 0 and t, the concentration of OTC is represented by C_0 and C_t, respectively, and the rate constant is represented by k_{obs}.

Results and Discussion

Catalyst Characterization

The SEM displayed that carbonized resin (CR) had a relatively smooth surface with a comparatively regular structure (Fig. 1 (a-d)). The surface of Fe_3O_4@CR existed tiny uniform particles with diameters of 100-150 nm (Fig. 1 (e-h)). After carbonization by doping with Fe, the smooth surface of the resin became rough attributed to the iron oxides adhering to the surface. The results proved that the iron oxide was successfully loaded onto CR.

The XRD of the Fe_3O_4@CR and CR was investigated in Fig. 2a). There was a distinct peak at 21.1° in the XRD spectrum of Fe_3O_4@CR and CR, which showed amorphous carbon diffraction peaks [23]. In Fe_3O_4@CR, the peaks at 18.45°, 30.36°, 35.76°, 43.47°, 57.51°, and 63.16° were indexed to (012), (220), (311), (400), (422), (440) planes of Fe_3O_4 (JCPDS PDF#75-0449), which indicated the Fe_3O_4 combination with the CR [24]. The XRD result further revealed the effective combination of Fe_3O_4 and CR in the calcination process. In Fig. 2b), there was a broad adsorption peak of Fe_3O_4@CR between 2900 cm^{-1} and 3700 cm^{-1}, which connected the typical bands of the -OH group [25]. At the other position, i.e., around 1125 cm^{-1} and 1622 cm^{-1}, the existing adsorption peak may be related to the C-O vibration [26]. Comparing with the peaks between 530 cm^{-1} and 540 cm^{-1}, it can be found that the obvious peak of Fe_3O_4@CR corresponded to the stretching of Fe-O bond, further indicating the presence of iron species in Fe_3O_4@CR [27]. As can be seen from

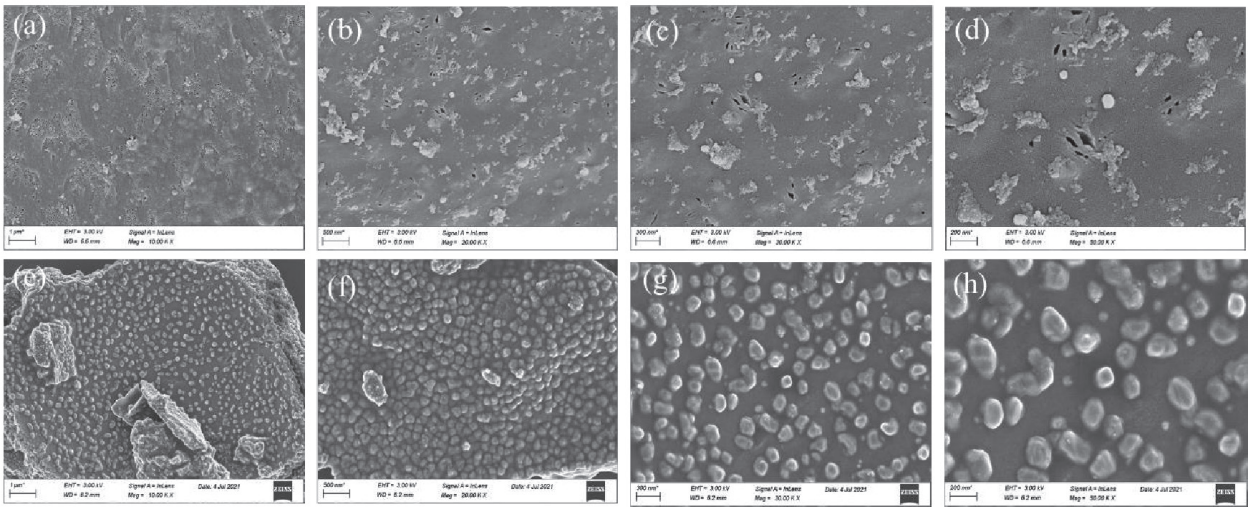

Fig. 1. SEM images of CR (a, b, c, d) and Fe_3O_4@CR (e, f, g, h) samples in different magnifications.

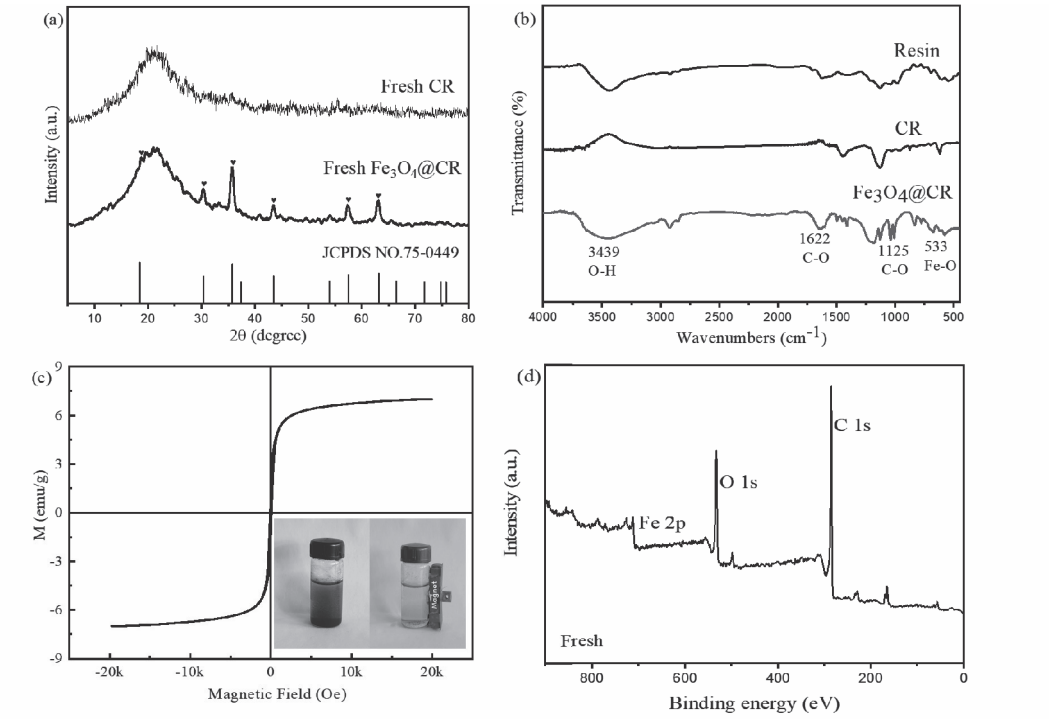

Fig. 2. The XRD patterns of Fe_3O_4@CR a); the FT-IR spectra of Fe_3O_4@CR b); the magnetic hysteresis loops for Fe_3O_4@CR c) and survey spectra XPS spectra of Fe_3O_4@CR d).

Fig. 2c), Fe_3O_4@CR had a saturation magnetization of nearly 7.7 emu/g, so it can be separated from the mixture with the help of a magnet. In Fig. 2d), the XPS measurement spectrum therein showed the main component of Fe_3O_4@CR, from which it was found that Fe was present.

The Catalytic Performance of Fe_3O_4@CR

In the only PS system, OTC showed no obvious degradation (Fig. 3a). In the only Fe_3O_4@CR system, about 20% of OTC was removed by adsorption. In terms of OTC degradation rate, the CR/PS system and Fe_3O_4/PS system were 17% and 31.9%, respectively. While the removal of OTC achieved 76.4% in the Fe_3O_4@CR/PS system, indicating the synergistic enhancement of catalytic performance after the doping of Fe in the CR. The enhanced catalytic performance of Fe_3O_4@CR may be due to the influence of its active components [27, 28]. In terms of OTC removal rate, the two systems mentioned above were 76.4% and 31.9% respectively, which were shown in Fig. 3a. 20% of PS was consumed in the Fe_3O_4/PS system, while 55% of PS consumption in the Fe_3O_4@CR/PS system (Fig. 3b). The result indicated that 35% of PS was consumed by CR, and the phenomenon presented synergistic catalytic effect after introducing CR to Fe_3O_4 [28].

The effect of Fe_3O_4@CR dosage on OTC removal was shown in Fig. 3c). The removal of OTC increased with the increase of Fe_3O_4@CR dosage. When the dosage of Fe_3O_4@CR was increased from 0 g/L to 0.3 g/L, the removal of OTC increased from 9.8% to 76.4% and the k_{obs} increased from 0.0023 min^{-1} to 0.0068 min^{-1} in Fig. 3d). However, when the dosage of Fe_3O_4@CR was 0.3 g/L - 0.4 g/L, the removal of OTC was not increased. This result indicated that Fe_3O_4@CR was fully utilized and the excess PS probably would not be activated anymore to bring about an increase in free radicals [29]. The superfluous Fe_3O_4@CR increased the active sites and produced a large amount of $SO_4^{\bullet-}$ in a short period, which speeded up the removal of OTC in the initial [30]. As shown in Fig. 3e), the influence of PS dosage on the reaction was studied. As the PS dosage increased from 0 g/L to 0.15 g/L, the removal of OTC increased from 10.4 % to 76.4 % and the k_{obs} increased from 0.0027 min^{-1} to 0.0074 min^{-1} in Fig. 4f). As the PS dosage was further increased from 0.15 g/L to 0.2 g/L, the removal of OTC was not significantly increased and the k_{obs} decreased from 0.0074 min^{-1} to 0.0070 min^{-1}. The decreased k_{obs} was related to the over-occupied sites of Fe_3O_4@CR. Excess $SO_4^{\bullet-}$ could be eliminated by each other, resulting in the decrease in the degradation process [31].

Temperature is an important factor for activating PS to degrade OTC. The OTC degradation at various temperatures can be seen in Fig. 3g). The high temperature in the reaction process can promote the reaction between the PS and Fe_3O_4@CR [32]. The correlation ($R^2 = 0.9284$) between 1/T and lnK was fitted with the Arrhenius equation and the apparent activation energy (E_a) was 28.86 kJ/mol (Fig. 3h). Compared with the catalysts of nZVI/BC (43.45 kJ/mol) [30], Porous Fe_2O_3 (69.22 kJ/mol) [33], the relatively lower E_a value proved that the reaction could be easily carried out.

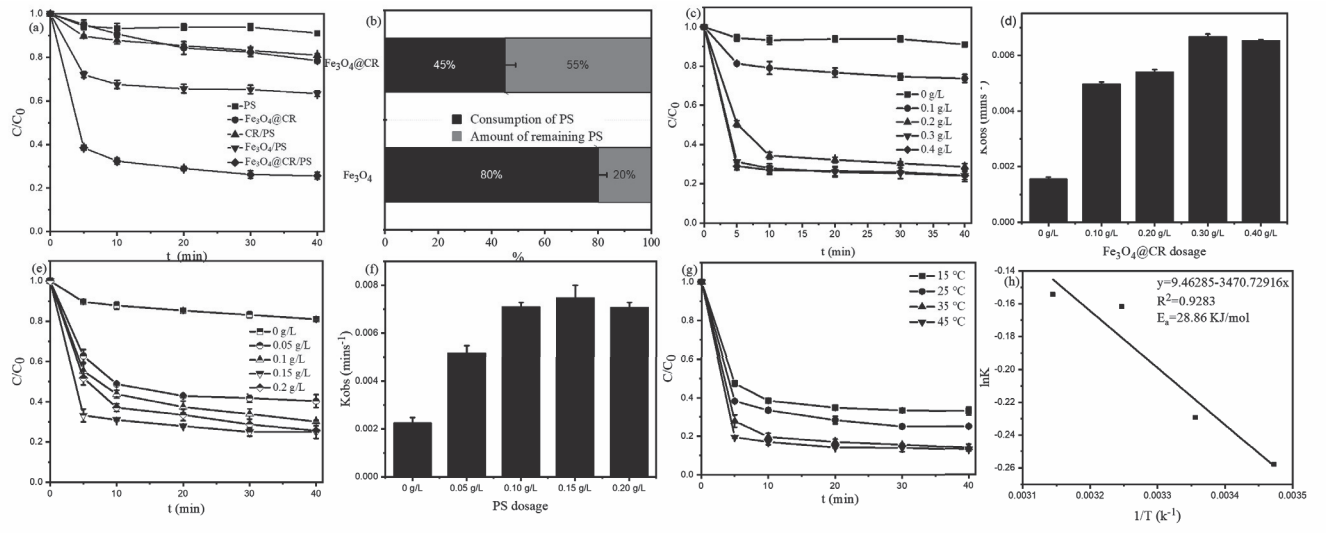

Fig. 3. The removal of OTC by PS, Fe_3O_4@CR, CR/PS, Fe_3O_4/PS, and Fe_3O_4@CR/PS system a) and the consumption of PS by Fe_3O_4/PS and Fe_3O_4@CR/PS system b); Effect of catalyst dosage c); PS dosage (e); and their kinetic rates (d, f) of OTC degradation corresponding to a, c respectively; effect of temperature (g) and the lnK vs. 1/T (h) (Experimental conditions: initial [OTC] = 20 mg/L, [Fe_3O_4@CR] = 0.3 g/L (except a), [PS] = 0.15 g/L (except c), T = 25ºC, without pH adjustment).

The result further indicated that the Fe_3O_4@CR owned potential catalytic activity on OTC degradation.

Effect of pH

As can be seen from Fig. 4a), when the solution was under the neutral and acidic pH range, OTC had a stable degradation rate, while the degradation was inhibited under alkaline condition. It was beneficial for OTC removal in acidic condition, which was due to the leaching of iron ions [34]. In alkaline conditions, the sedimentation of iron ions was expedited and coated on the surface, causing an adverse effect on activating PS (Eq. (2)) [35]. After the reaction was complete,

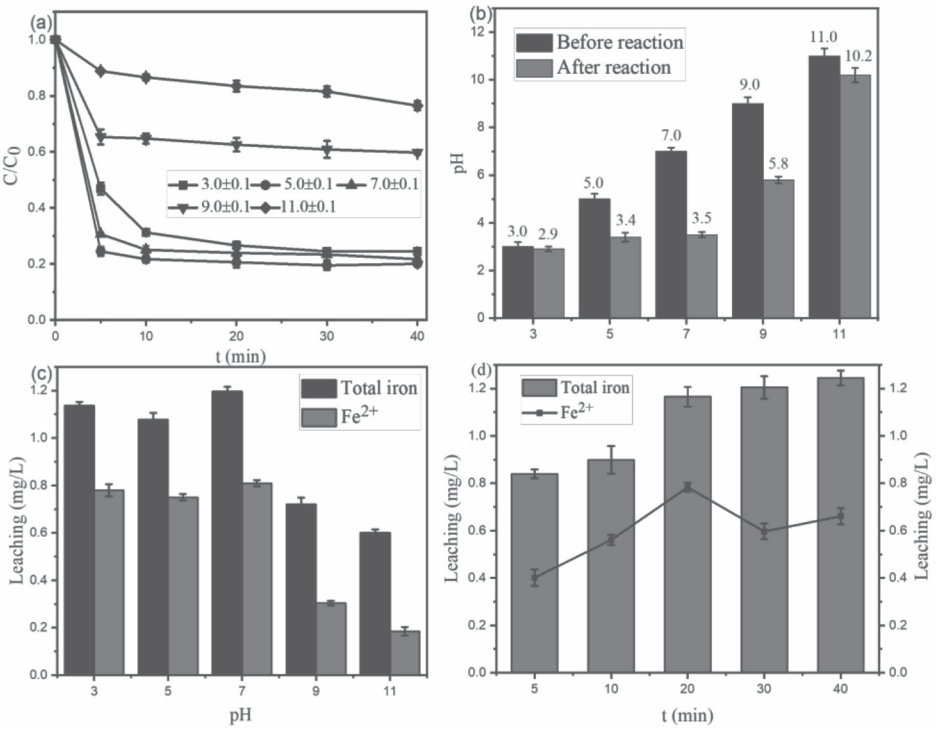

Fig. 4. Effect of initial pH on OTC degradation a); the pH value before and after reaction b); the leaching of Fe ions in different pH c); and the optimal conditions during the OTC degradation process d) (Experimental conditions: initial [OTC] = 20 mg/L, [Fe_3O_4@CR] = 0.3 g/L, [PS] = 0.15 g/L, T =25ºC).

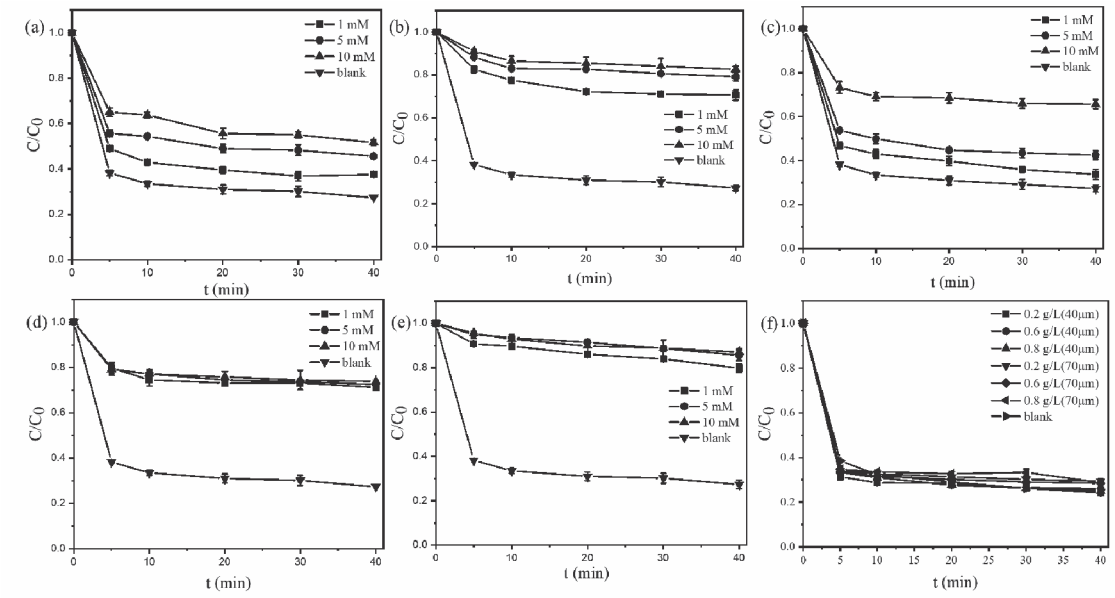

Fig. 5. Effect of coexisting anions (1 mM, 5 mM and 10 mM) in Fe_3O_4@CR/PS system: a) Cl^-; b) $H_2PO_4^-$; c) SO_4^{2-}; d) HCO_3^-; e) CO_3^{2-} and f) Microplastics (Experimental conditions: [OTC] = 20 mg/L, [Fe_3O_4@CR] = 0.3 g/L, [PS] = 0.15 g/L, T = 25ºC).

the pH of the solution was acidic (except the initial pH = 11.0) (Fig. 4b). The H^+ byproduct was produced via PS decomposing, resulting in the decrease of pH value [36]. The leaching of the total Fe at pH values of 3.0, 5.0, 7.0, 9.0, 11.0 was 1.13 mg/L, 1.07 mg/L, 1.19 mg/L, 0.72 mg/L, and 0.60 mg/L, respectively (Fig. 4c). The higher leaching concentration was consistent with the better degradation performance under the neutral and acidic pH range [27]. The leaching of total Fe and Fe^{2+} in the reaction process was shown in Fig. 5d). The leaching of total Fe was increased as the time increased, and the Fe^{2+} was increased at the early stage and then decreased in the reaction. The results indicated that the valence of iron changed in the degradation process [28]. Fig. 4d) showed that the leaching of Fe^{2+} was reacted with $SO_4^{\bullet-}$ and produced Fe^{3+} in the solution (Eq. (3)) [37].

$$S_2O_8^{2-} + Fe^{2+} \rightarrow SO_4^{\bullet-} + SO_4^{2-} + Fe^{3+} \quad (2)$$

$$Fe^{2+} + SO_4^{\bullet-} \rightarrow Fe^{3+} + SO_4^{2-} \quad (3)$$

Effect of Coexisting Pollutants and Reusability of Fe_3O_4@CR

Fig. 5 showed the removal of OTC with the co-existing anions and microplastics in the Fe_3O_4@CR/PS system. Here, the degradation was affected by Cl^-, because of its quenching effect on $SO_4^{\bullet-}$ (Eq. (4)) [38]. The existence of $H_2PO_4^-$ indicated a negative effect and the removal of OTC was only 17.3% as the dosage of $H_2PO_4^-$ was 10 mM. The active sites of Fe_3O_4@CR may be occupied by $H_2PO_4^-$, and the activation of PS was inhibited [39]. SO_4^{2-} had an inhibition effect on the OTC degradation. The SO_4^{2-} could reduce the oxidation-reduction potential of $SO_4^{\bullet-}/SO_4^{2-}$, which leads to the inhibition of activation [40]. Generally, HCO_3^- had a negative effect on the degradation process because of its free radical quencher. HCO_3^- could quench $SO_4^{\bullet-}$ and $^{\bullet}OH$ to produce less reactive carbonate radical ($CO_3^{\bullet-}/HCO_3^{\bullet-}$) (Eqs (5)-(7)) [41]. The existence of CO_3^{2-} showed a similar effect as the existence of HCO_3^- because they were converted to each other (Eq. (8)) [42]. Obviously, microplastics showed no effect on the degradation process, which demonstrated that the Fe_3O_4@CR/PS had a potential for OTC degradation in the presence of microplastics.

$$SO4^{\bullet-} + Cl^- \rightarrow SO_4^{2-} + Cl^{\bullet} \quad (4)$$

$$\bullet OH + HCO_3^- \rightarrow CO_3^{\bullet-} + H_2O \quad (5)$$

$$SO4^{\bullet-} + HCO_3^- \rightarrow SO_4^{2-} + HCO_3^{\bullet-} \quad (6)$$

$$HCO_3^{\bullet-} \leftrightarrow H^+ + CO_3^{\bullet-} \quad (7)$$

$$HCO_3^- \leftrightarrow H^+ + CO_3^{2-} \quad (8)$$

Proposed Degradation Mechanisms

As can be seen from Fig. 6a), the OTC degradation efficiency decreased from 76.4% to 22.1% in the presence of MeOH. The removal of OTC was 56.9 % in the presence of TBA. When chlorine and L-histidine were present, there was a negligible effect on the removal of OTC. MeOH and TBA had a great impact on the degradation, indicating that $SO_4^{\bullet-}$ and $^{\bullet}OH$ radicals played a vital role in OTC degradation in the Fe_3O_4@CR/PS system. To further confirm the generated $SO_4^{\bullet-}$ and $^{\bullet}OH$ radicals in the Fe_3O_4@CR/PS system, EPR

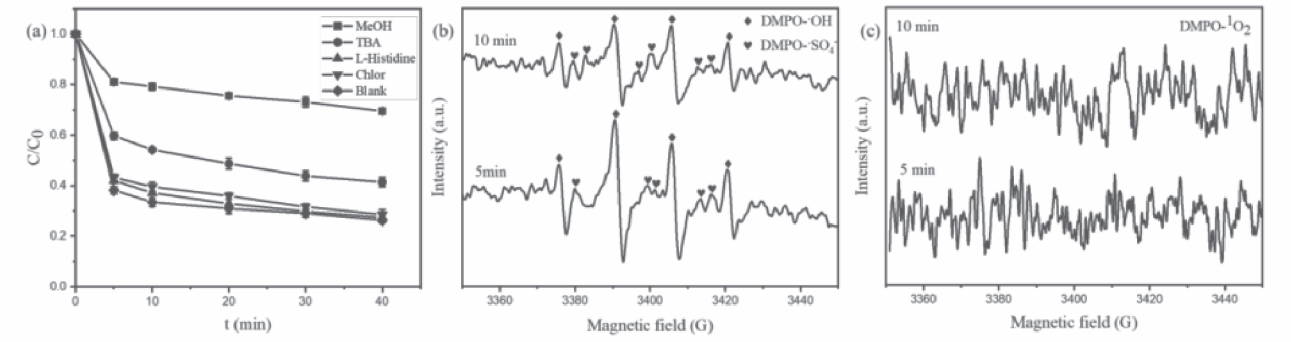

Fig. 6. The effect of radical scavengers on OTC degradation in the Fe_3O_4@CR/PS system (a); DMPO spin trapping EPR spectra (b, c) (Experimental conditions: initial [OTC] = 20 mg/L, [Fe_3O_4@CR] = 0.3 g/L, [PS] = 0.15 g/L, T = 25ºC, without pH adjustment, [MeOH]: [PS] = 200:1, [TBA]: [PS] =200:1, [L-histidine]: [PS] =200:1, [Chlor]: [PS] =200:1, [DMPO] = 10 mM, [TEMP] = 10 mM).

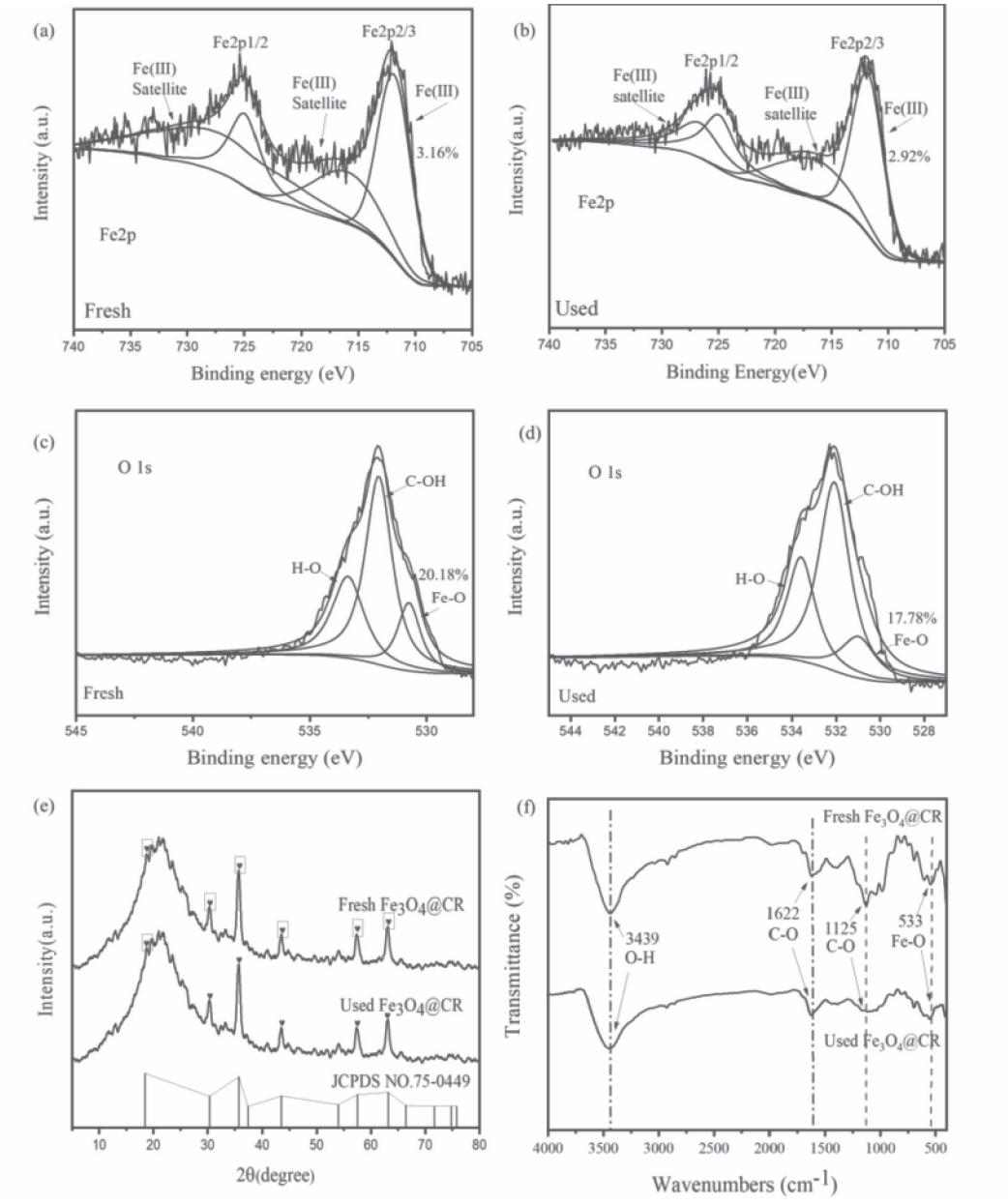

Fig. 7. XPS spectra of fresh and used Fe_3O_4@CR: Fe2p (a, b), O1s (c, d); The XRD patterns (e) and FT-IR spectra of fresh Fe_3O_4@CR and used Fe_3O_4@CR (b) (Experimental conditions: initial [OTC] = 20 mg/L, [Fe_3O_4@CR] = 0.3 g/L, [PS] = 0.15 g/L, T = 25ºC, without pH adjustment).

was carried out in Fig. 6(b, c). The presence of DMPO-$SO_4^{\bullet-}$ and DMPO-$^{\bullet}OH$ signal indicated the production of $SO_4^{\bullet-}$ and $^{\bullet}OH$ in the reaction system. The drop of $SO_4^{\bullet-}$ and •OH radicals signal at 5-10 minutes was due to the high consumption, which indicated that $SO_4^{\bullet-}$ and •OH were the major reactive species for OTC degradation. The characteristic signal of $^1O_2$ was not discovered, indicating that $^1O_2$ was not involved in the reaction.

The XPS spectra of Fe2p and O1s showed that the Fe-O function group and Fe ions were consumed in the Fe_3O_4@CR/PS system (Fig. 7a-d). The content of Fe^{3+} reduced from 3.16% to 2.92%, and the content of the Fe-O function group reduced from 20.18% to 17.78%. The decrease in Fe^{3+} content indicated that Fe^{3+} was consumed in the degradation process. It indicated that the leaching of Fe^{3+} activated PS to degrade OTC in the Fe_3O_4@CR/PS system. The decrease of Fe-O indicated that Fe-O was the major active site on the surface of Fe_3O_4@CR [28]. During the OTC degradation, the generated acidic chemicals enhanced the acidity of the solution and resulting in Fe^{3+} leaching [43]. The $SO_4^{\bullet-}$ was generated in the reaction during the conversion of Fe^{3+} to Fe^{2+}, and the $HO^{\bullet}$ was generated by the reaction between $SO_4^{\bullet-}$ and H_2O. The addition of iron increased the surface area of CR and improved the adsorption of OTC on the surface of Fe_3O_4@CR. Moreover, the XRD patterns and FT-IR spectra of Fe_3O_4@CR after the reaction demonstrated that the catalysts were stable (Fig. 7e-f). The functional groups on the Fe_3O_4@CR were analyzed by XRD in Fig. 7e). After the reaction, the structure of Fe_3O_4@CR exhibited no obvious difference, demonstrating that the materials were stable. FTIR also proved the stability of Fe_3O_4@CR in the reaction process (Fig. 7f). The stability performance indicated that the catalyst owned a great potential to activate PS.

And the relevant chemical equations were Eqs (9-13).

$$Fe^{3+} + S_2O_8^{2-} \rightarrow Fe^{2+} + S_2O_8^{\bullet-} \quad (9)$$

$$Fe^{2+} + S_2O_8^{2-} \rightarrow Fe^{3+} + SO_4^{\bullet-} + SO_4^{2-} \quad (10)$$

$$SO_4^{\bullet-} + H_2O \rightarrow SO_4^{2-} + {}^{\bullet}OH + H^+ \quad (11)$$

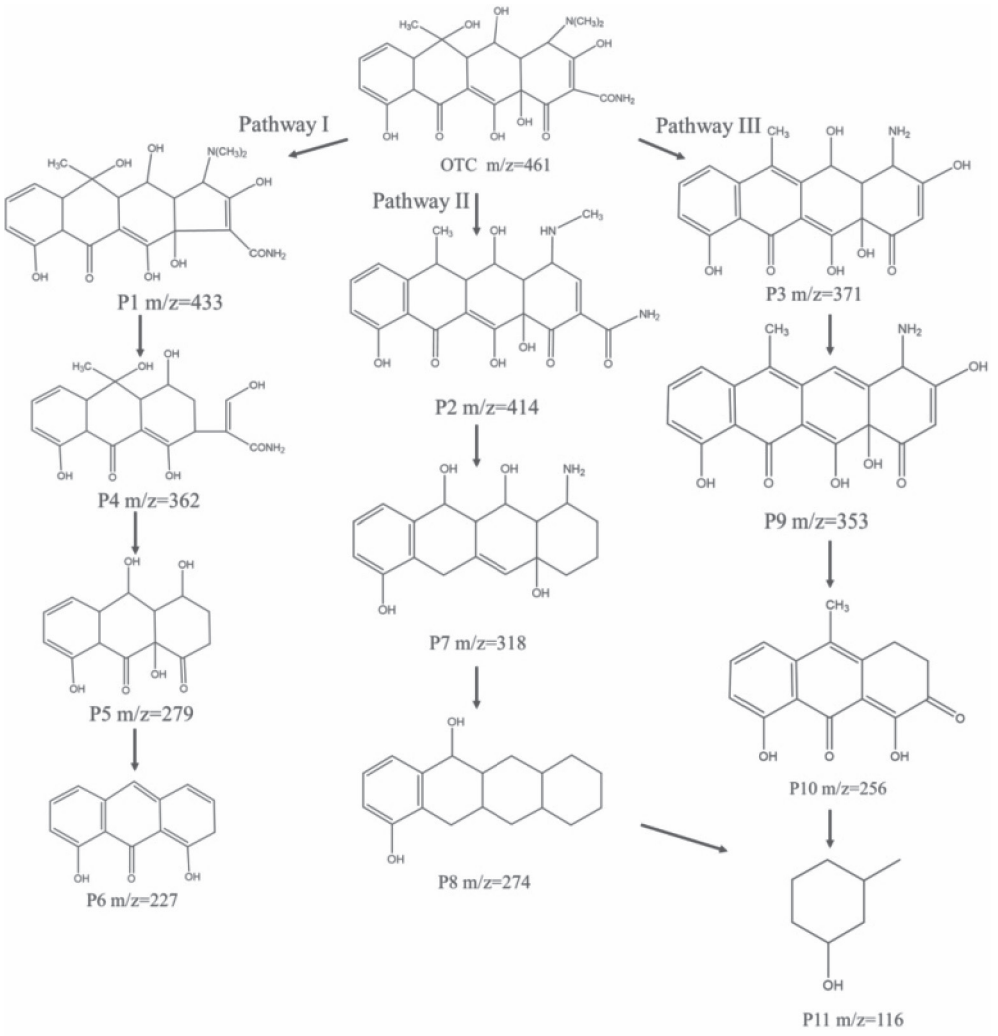

Fig. 8. Possible degradation pathways for OTC

$$HSO_5^- + OH^- \rightarrow SO_5^{\bullet-} + H_2O \quad (12)$$

$$HSO_5^- + SO_4^{\bullet-} \rightarrow SO_5^{\bullet-} + H^+ \quad (13)$$

OTC Degradation Intermediates and Possible Pathways

The mineralization products were further studied and the possible pathways of OTC degradation were displayed in Fig. 8. The degradation pathway of OTC mainly included demethylation, decarbonylation, deoxidation and ring-opening [44]. The •OH active species could attack the aromatic ring of OTC in the Fe_3O_4@CR/PS system [44]. P1 (m/z = 433) could be obtained after decarbonylation from the OTC ring. When the ring-opening reaction of P1 occurred and the N-methyl group was eliminated at the same time, P4 (m/z = 362) will appear. Based on this, the methyl group, carbon group and amino group will be removed to obtain P5 (m/z = 279). P5 was further decomposed by •OH to produce aliphatic compounds, such as P6 (m/z = 227) [45]. Then two hydroxyl groups were removed in OTC, and P2 (m/z = 414) was obtained. The methyl group, carbon group and amino group of P2 were removed to obtain P7 (m/z = 318) [46], and the amino group and hydroxyl group were further removed to obtain P8 (m/z = 274). While in OTC, P3, P9 and P10 can be obtained by removal of hydroxyl and N-methyl, dehydration, decarboxylation, and dehydration during degradation, respectively. During this process, the intermediates P8 and P10 were oxidized to produce some byproducts (such as P11 (m/z = 116)) that undergo dehydration, ring-opening, and demethylation reactions [47]. Finally, the intermediate products of OTC were further mineralized to smaller molecules, even H_2O and CO_2.

Conclusions

The Fe_3O_4@CR was synthesized and applied in the activated persulfate for the degradation of OTC. Around 76.4 % of OTC was degraded at the conditions ([PS]: 0.15 g/L, [Fe_3O_4@CR]: 0.3 g/L, T: 25ºC). When the pH value was between 3.0 and 7.0, the Fe_3O_4@CR/PS system can function effectively. Co-existing ions had a negative effect on OTC removal in the Fe_3O_4@CR/PS system, while co-existing microplastics proved no effect. The key reactive radical for OTC degradation was $SO_4^{\bullet-}$ and •OH. The conversion between Fe^{3+} and Fe^{2+} enhanced the degradation and the possible degradation pathways were proposed. The OTC was mineralized to smaller molecules ($C_{14}H_{10}O_3$, $C_7H_{11}O$) by means of three ways. This work presented a stable and high-activity catalyst for the removal of OTC and provided an alternative approach for the reuse of waste cation exchange resin.

Acknowledgments

We gratefully acknowledge the generous support provided by the "National Natural Science Foundation of China (51908432)", the "Natural Science Foundation of Hubei Province (2018CFB397)," and the "Central Government Guides Local Science and Technology Development Special Program (2022BGE273)", China". We also would like to thank Shiyanjia Lab (www.shiyanjia.com) for the SEM, TEM, FTIR, XPS, EPR analysis.

Conflict of Interest

The authors declare that they have no known competing financial interests or personal relationships that could have appeared to influence the work reported in this paper.

References

1. DONG F., YAN L., HUANG S., LIANG J., ZHANG W., YAO X., CHEN X., QIAN W., GUO P., KONG L., CHU W., DIAO Z. Removal of antibiotics sulfadiazine by a biochar based material activated persulfate oxidation system: Performance, products and mechanism, Process Saf. Environ. **157** (1), 411, **2021**.
2. DIAO Z.H., JIN J.C., ZOU M.Y., LIU H., QIN J.Q., ZHOU X.H., QIAN W., GUO P.R., KONG L.J., CHU W. Simultaneous degradation of amoxicillin and norfloxacin by TiO_2@nZVI composites coupling with persulfate: Synergistic effect, products and mechanism, Sep. Purif. Technol. **278** (12), 119620, **2021**.
3. FENG C., LU Z.W., ZHANG Y.Z., LIANG Q., ZHOU M., LI X.Z., YAO C., LI Z.Y., XU S. A magnetically recyclable dual Z-scheme GCNQDs-$CoTiO_3$/$CoFe_2O_4$ composite photocatalyst for efficient photocatalytic degradation of oxytetracycline. Chem. Eng. J. **435** (1), 134833, **2022**.
4. DENG J., SHAO Y., GAO N., DENG Y., ZHOU S., HU X. Thermally activated persulfate (TAP) oxidation of antiepileptic drug carbamazepine in water. Chem. Eng. J. **228** (7), 765, **2013**.
5. GAO Y., WANG Q., JI G. Degradation of antibiotic pollutants by persulfate activated with various carbon materials, Chem. Eng. J. **429** (2), 132387, **2022**.
6. LI Q., PAN F., LI W., LI D., XU H., XIA D., LI A. Enhanced adsorption of bisphenol A from aqueous solution with 2-vinylpyridine functionalized magnetic nanoparticles. Polymers. **10** (10), 1136, **2018**.
7. GAO Y., ZHOU Y., PANG S.Y., JIANG J., YANG Z., SHEN Y., WANG Z., WANG P.X., WANG L.H. New insights into the combination of permanganate and bisulfite as a novel advanced oxidation process: importance of high valent manganese-oxo species and sulfate radical. Environ. Sci. Technol. **53** (7), 3689, **2019**
8. HUANG H., GUO T., WANG K., LI Y., ZHANG G. Efficient activation of persulfate by a magnetic recyclable rape straw biochar catalyst for the degradation of tetracycline hydrochloride in water. Sci. Total Environ. **758**, 143957, **2021**.

9. PAN X., CHEN J., WU N., QI Y., XU X., GE J., WANG X., LI C., QU R., SHARMA V.K., WANG Z. Degradation of aqueous 2,4,4′-Trihydroxybenzophenone by persulfate activated with nitrogen doped carbonaceous materials and the formation of dimer products. Water Res. **143**, 176-187, **2018**.
10. GRAçA C., VELOSA A., TEIXEIRA A. Amicarbazone degradation by UVA-activated persulfate in the presence of hydrogen peroxide or Fe^{2+}. Catal. Today. **280** (2), 80, **2017**.
11. YE Y., WAN J., LI Q., HUANG Y., PAN F., Xia D. Catalytic oxidation of dyeing wastewater by copper oxide activating persulfate: performance, mechanism and application, Int. J. Environ. Res. **15** (1), 1, **2021**.
12. SI J., YANG X., LUAN H., SHAO Y., YAO K. Cheap, fast and durable degradation of azo dye wastewater by zero-valent iron structural composites. J. Environ. Chem. Eng. **9** (5), 106314, **2021**.
13. MAHLAULE-GLORY L.M., MAPETLA S., MAKOFANE A., MATHIPA M.M., HINTSHO-MBITA N.C. Biosynthesis of iron oxide nanoparticles for the degradation of methylene blue dye, sulfisoxazole antibiotic and removal of bacteria from real water. Heliyon. **8** (9), e10536, **2022**.
14. MAHMOUDABADI Z.S., RASHIDI A., MAKLAVANY D.M. Optimizing treatment of alcohol vinasse using a combination of advanced oxidation with porous α-Fe_2O_3 nanoparticles and coagulation-flocculation. Ecotox. Environ. Safe. **234**, 113354, **2022**.
15. LI X., QIN Y., JIA Y., LI Y., SUN J. Preparation and application of Fe/biochar (Fe-BC) catalysts in wastewater treatment: A review. Chemosphere. **274** (7), 129766, **2021**.
16. GUO J., JIANG J., CHEN Y., WEN X., CHEN W., WANG Y., SU L., CAO J. Synthesis of nZVI-BC composite for persulfate activation to degrade pyrene: Performance, correlative mechanisms and degradation pathways, Process Saf. Environ. **162**, 733, **2022**.
17. YU Y., LI N., WANG C., CHENG Z., YAN B., CHEN G., HOU L.A., WANG S. Iron cobalt and nitrogen co-doped carbonized wood sponge for peroxymonosulfate activation: Performance and internal temperature-dependent mechanism. J. Colloid. Interf. Sci. **619**, 267, **2022**.
18. YANG L., WEI Y., PENG Y., LIU Y., SHU Z., WANG Y., MENG Q., ZHAO C., ZHAO H., YANG F., LAI B. Carbonized resin with Fe&Co bimetal for peroxymonosulfate activation to degrade atrazine. Sep. Purif. Technol. **292**, 121049, **2022**.
19. LIU Z., WANG L., LV Y., XU X., ZHU C., LIU F., LI A. Impactful modulation of micro-structures of acid-resistant picolylamine-based chelate resins for efficient separation of heavy metal cations from strongly acidic media. Chem. Eng. J. **420**, 129684, **2021**.
20. LIU Y., GUO H.G., ZHANG Y.L., CHENG X., ZHOU P., WANG J.Q., LI W. Fe@C carbonized resin for peroxymonosulfate activation and bisphenol S degradation. Environ. Pollut. **252** (9), 1042, **2019**.
21. SHI Q., LI A., QING Z., LI Y. Oxidative degradation of Orange G by persulfate activated with iron-immobilized resin chars. J. Ind. Eng. Chem. **25** (5), 308, **2015**.
22. Y. LIU, H.GUO, Y. ZHANG, XIN C., PENG Z., JING D., JINGQUAN W., WEI L. Highly efficient removal of trimethoprim based on peroxymonosulfate activation by carbonized resin with Co doping: Performance, mechanism and degradation pathway. Chem. Eng. J. **356** (15), 717, **2018**.
23. BELIN T., EPRON F. Characterization methods of carbon nanotubes: a review. Mat. Sci. Eng. B. **119** (2), 105, **2005**.
24. ANIPSITAKIS G.P., DIONYSIOU D.D. Radical generation by the interaction of transition metals with common oxidants, Environ. Sci. Technol. **38** (13), 3705, **2004**.
25. CAO J., YANG Z., XIONG W., ZHOU Y., WU Y., JIA M., SUN S., ZHOU C., ZHANG Y., ZHONG R. Peroxymonosulfate activation of magnetic Co nanoparticles relative to an N-doped porous carbon under confinement: Boosting stability and performance, Sep. Purif. Technol. **250**, 117237, **2020**.
26. ZHU K., BIN Q., SHEN Y., AL. E. In-situ formed N-doped bamboo-like carbon nanotubes encapsulated with Fe nanoparticles supported by biochar as highly efficient catalyst for activation of persulfate (PS) toward degradation of organic pollutants. Chem. Eng. J. **402** (12), 126090, **2020**.
27. TONG J., CHEN L., CAO J., YANG Z., XIONG W., JIA M., XIANG Y., PENG H. Biochar supported magnetic MIL-53-Fe derivatives as an efficient catalyst for peroxydisulfate activation towards antibiotics degradation. Sep. Purif. Technol. **294** (4), 121064, **2022**.
28. SONG H., LI Q., YE Y., PAN F., XIA D. Degradation of cephalexin by persulfate activated with magnetic loofah biochar: Performance and mechanism. Sep. Purif. Technol. **272** (10), 118971, **2021**.
29. JUAN H., JINGCHUN T., ZHENG Z., LAN W., QINGLONG L., XIAOMEI L. Magnetic ball-milled FeS@biochar as persulfate activator for degradation of tetracycline. Chem. Eng. J. **404** (1), 126997, **2021**.
30. HUSSAIN I., LI M., ZHANG Y., LI Y., HUANG S., DU X., LIU G., HAYAT W., ANWAR N. Insights into the mechanism of persulfate activation with nZVI/BC nanocomposite for the degradation of nonylphenol. Chem. Eng. J. **311** (3), 163, **2017**.
31. PAN X., WEI J., ZOU M., CHEN J., QU R., WANG Z. Products distribution and contribution of (de) chlorination, hydroxylation and coupling reactions to 2, 4-dichlorophenol removal in seven oxidation systems. Water Res. **194**, 116916, **2021**.
32. HO S.-H., CHEN Y., LI R., ZHANG C. N-doped graphitic biochars from C-phycocyanin extracted spirulina residue for catalytic persulfate activation toward nonradical disinfection and organic oxidation. Water Res. **159** (8), 77, **2019**.
33. JI F., LI C., WEI X., YU J., Efficient performance of porous Fe_2O_3 in heterogeneous activation of peroxymonosulfate for decolorization of Rhodamine B. Chem. Eng. J. **231**, 434, **2013**.
34. DING D., LIU C., JI Y., QIAN Y., CAI T. Mechanism insight of degradation of norfloxacin by magnetite nanoparticles activated persulfate: Identification of radicals and degradation pathway. Chem. Eng. J. **308** (1), 330, **2017**.
35. NGUYEN V.T., HUNG C.M., NGUYEN T.B., CHANG J.H., WANG T.H., WU C.H., LIN Y.L., CHEN C.W., DONG C.D. Efficient heterogeneous activation of persulfate by Iron-modified biochar for removal of antibiotic from aqueous solution: a case study of tetracycline removal. Catalysts. **49** (1), **2019**.
36. ZHANG D., SUN J., LI Q., SONG H., XIA D. Cu-Doped magnetic loofah biochar for tetracycline degradation via peroxymonosulfate activation. New J. Chem. **46** (36), 17223, **2022**.
37. CAO J., LAI L., LAI B., YAO G., CHEN X., SONG L. Degradation of tetracycline by peroxymonosulfate

activated with zero-valent iron: Performance, intermediates, toxicity and mechanism. Chem. Eng. J. **364** (5), 45, **2019**.

38. OUTSIOU A., FRONTISTIS Z., RIBEIRO R.S., ANTONOPOULOU M., KONSTANTINOU I.K., SILVA A.M.T., FARIA J.L., GOMES H.T., MANTZAVINOS D. Activation of sodium persulfate by magnetic carbon xerogels (CX/CoFe) for the oxidation of bisphenol A: Process variables effects, matrix effects and reaction pathways. Water Res. **124** (11), 97, **2017**.
39. WANG L., JIANG J., PANG S.Y., ZHOU Y., JIANG C. Oxidation of bisphenol A by nonradical activation of peroxymonosulfate in the presence of amorphous manganese dioxide. Chem. Eng. J. **352** (11), 1004, **2018**.
40. ZHOU T., ZOU X., MAO J., WU X. Decomposition of sulfadiazine in a sonochemical Fe0-catalyzed persulfate system: Parameters optimizing and interferences of wastewater matrix. Appl. Catal. B: Environ. **185** (5), 31, **2016**.
41. LI Z., SONG W., CHEN Z., YIN G. Degradation of organic pollutants in wastewater by bicarbonate-activated hydrogen peroxide with a supported cobalt catalyst. Environ. Sci. Technol. **47** (8), 3833, **2013**.
42. SUN J., LI Q., ZHANG D., XIA D. Relying on the non-radical degradation of oxytetracycline by peroxymonosulfate activated with a magnetic Cu/Fe composite: performance and mechanism. New J. Chem. **46** (38), 18251, **2022**.
43. HAYON E., TREININ A., WILF J. Electronic spectra, photochemistry, and autoxidation mechanism of the sulfite-bisulfite-pyrosulfite systems. SO_2-, SO_3-, SO_4-, and SO_5-radicals, J. Am. Chem. Soc. **94**, 47, **1972**.
44. YAN T., PING Q., ZHANG A., WANG L., DOU Y., LI Y. Enhanced removal of oxytetracycline by UV-driven advanced oxidation with peracetic acid: Insight into the degradation intermediates and N-nitrosodimethylamine formation potential. Chemosphere. **274**, 129726, **2021**.
45. GUSAIN R., KUMAR N., OPOKU F., GOVENDER P.P., RAY S.S. MoS_2 nanosheet/ZnS composites for the visible-light-assisted photocatalytic degradation of oxytetracycline. ACS Appl. Nano Mater. **4** (5), 4721, **2021**.
46. LIU X., PEI Y., CAO M., YANG H., LI Y. Highly dispersed copper single-atom catalysts activated peroxymonosulfate for oxytetracycline removal from water: Mechanism and degradation pathway. Chem. Eng. J. **450**, 138194, **2022**.
47. JIAO S., ZHENG S., YIN D., WANG L., CHEN L. Aqueous oxytetracycline degradation and the toxicity change of degradation compounds in photoirradiation process. J. Environ. Sci. **20** (7), 806, **2008**.